GA–A23698

ELECTRON CYCLOTRON WAVE EXPERIMENTS ON DIII–D

by

C.C. PETTY, J.S. deGRASSIE, R.W. HARVEY, Y.R. LIN-LIU,
J.M. LOHR, T.C. LUCE, M.A. MAKOWSKI, Y.A. OMELCHENKO,
and R. PRATER

JUNE 2001

DISCLAIMER

GA–A23698

ELECTRON CYCLOTRON WAVE EXPERIMENTS ON DIII–D

by
C.C. PETTY, J.S. deGRASSIE, R.W. HARVEY,† Y.R. LIN-LIU, J.M. LOHR, T.C. LUCE, M.A. MAKOWSKI,‡ Y.A. OMELCHENKO, and R. PRATER

†CompX
‡Lawrence Livermore National Laboratory

This is a preprint of a paper to be presented at the 14th Topical Conference on Applications of Radio Frequency Power to Plasmas, May 7–9, 2001, in Oxnard, California, and to be published in the *Proceedings.*

Work supported by
the U.S. Department of Energy
under Contracts DE-AC03-99ER54463, W-7405-ENG-48
and Grant DE-FG03-99ER54541

GA PROJECT 30033
JUNE 2001

Electron Cyclotron Wave Experiments on DIII–D

C.C. Petty,[1] J.S. deGrassie,[1] R.W. Harvey,[2] Y.R. Lin-Liu,[1] J.M. Lohr,[1] T.C. Luce,[1] M.A. Makowski,[3] Y.A. Omelchenko,[1] and R. Prater[1]

[1]*General Atomics, P.O. Box 85608, San Diego, California 92186*
[2]*CompX, Del Mar, California 92014-5672*
[3]*Lawrence Livermore National Laboratory, Livermore, California 94550*

Abstract: Electron cyclotron current drive (ECCD) experiments on the DIII–D tokamak are solidifying the physics basis for localized, off-axis current drive in both standard and advanced operating modes, the goal being to validate a predictive model for ECCD. The measured ECCD efficiency is found to be in agreement with theoretical calculations using the CQL3D Fokker-Planck code over a range of toroidal injection angles, absorption radii, and electron beta. The latter dependence is especially important since the ECCD efficiency is shown to increase with local electron beta, which is favorable for current profile control using off-axis ECCD in high-beta advanced tokamaks.

INTRODUCTION

Electron cyclotron waves offer the unique ability to probe and modify the transport and stability properties of magnetically confined plasmas. On the DIII–D tokamak, a versitile experimental program uses high power electron cyclotron waves to probe the transport properties, control MHD instabilities, and modify the plasma current profile. In addition, ongoing electron cyclotron current drive (ECCD) experiments are solidifying the physics basis for localized, off-axis current drive in both standard and advanced operating modes, the goal being to validate a predictive model of ECCD.

Previous experiments on DIII–D in low-density L–mode plasmas concentrated on validating the expected strong dependencies of the ECCD efficiency on electron trapping and the quasilinear effect [1–3]. The ECCD radial profile was determined from internal magnetic field measurements by motional Stark effect (MSE) spectroscopy either by comparing the total and ohmic current profiles determined by equilibrium reconstruction [1,2] or by comparing the measured MSE signals to simulations of the expected MSE response to localized current drive [3]. These local analysis methods differ from other ECCD experiments that inferred the global magnitude of the driven current from the change in the loop voltage at the plasma surface [4].

The experiments reported in this paper have extended the comparisons between ECCD experiment and theory to high-beta H–mode plasmas. Four gyrotrons are used in these experiments, with up to 2.1 MW of injected power. The gyrotrons operate at 110 GHz, which corresponds to the second harmonic of the electron cyclotron frequency at the plasma center. The electron cyclotron waves are launched from the low magnetic field side of the torus with X–mode polarization. The polarization of the launched wave is controlled by adjusting the inclination of grooved mirrors located in two mitre bends of the evacuated waveguide [5]. Experiments on DIII–D have verified the correct operation of the polarizers by scanning the inclination and ellipticity of the launched beam and measuring the unwanted O–mode component [6].

LOCALIZATION MEASUREMENTS

Advanced tokamak scenarios on DIII–D need narrow beams in nearly pure X–mode to achieve the requirement of highly localized deposition and current drive. Theoretically, the electron cyclotron waves should be strongly damped in the vicinity of the second harmonic electron cyclotron resonance. The absorption profile of electron cyclotron waves is determined by modulating the gyrotron power at 100 Hz and measuring the electron temperature (T_e) response using a 32-channel heterodyne radiometer [7]. In the limit of infinite modulation frequency (f), the temperature response ($\tilde{T}_e$) is everywhere proportional to the heating source with a 90° phase lag from the injected power. For square wave modulation, the power deposition profile can be found from [8]

$$P_{ec} = 6 f n_e \tilde{T}_e \quad , \tag{1}$$

where n_e is the electron density. However, this measurement places only an upper bound on the deposition profile width since energy transport effects are not negligible for the relatively low modulation frequency of 100 Hz used in these experiments.

Localized power deposition is measured for both L–mode plasmas and ELMing (edge localized mode) H–mode plasmas on DIII–D. The experimental and theoretical power deposition profiles are shown in Fig. 1(a) for a case of radial launch ($N_{||} = 0$, where $N_{||}$ is the parallel index of refraction). The theoretical deposition profile is calculated using the TORAY-GA ray tracing code [9,10]. Figure 1(a) shows that the measured and predicted deposition location and profile full width at half maximum (FWHM) are in good agreement (the wings of the measured deposition profile are due to the broadening effects of energy transport). A more stringent test of the ECH power deposition profile is shown in Fig. 1(b) for an ELMing H–mode plasmas with the resonance located near the midplane on the high magnetic field side of the torus. Two experimental cases are given, one for radial launch ($N_{||} = 0$) and one for co current drive launch ($N_{||} = 0.4$). The change in the deposition location for these two $N_{||}$ values due to

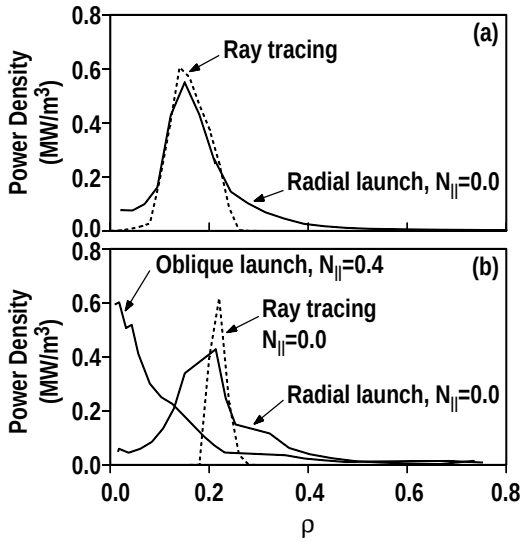

Fig. 1. Experimental (solid lines) and theoretical (dashed lines) ECH power deposition profiles for (a) L–mode plasma with radial launch (B_T=2.0 T), and (b) ELMing H–mode plasma with both radial and oblique launch with the resonance on the high field side of the plasma axis (B_T=1.9 T).

the Doppler effect is apparent in this figure. The theoretical power deposition profile is quite narrow because of the magnetic geometry for high field deposition, as shown in Fig. 1(b) for the radial launch case. Although the measured power deposition profile is not quite this narrow, probably due to energy transport effects, the experimental profile is still localized with a FWHM of ≈ 10% of the plasma minor radius.

Measurements using MSE spectroscopy [11] show that the increase in current density from ECCD is as localized as ray tracing calculations predict. Figure 2(a) shows the change in the channel-to-channel differences in the vertical magnetic field measured by MSE for ELMing H–mode plasmas with and without ECCD, *i.e.*

$$\Delta \frac{1}{\mu_o} \frac{\partial B_z}{\partial R} \propto \Delta J_\phi \quad , \tag{2}$$

where B_z is the vertical magnetic field, R is the major radius, and J_ϕ is the toroidal current density. The theoretical location and width of the ECCD, calculated by the TORAY-GA code, is also indicated in this figure. The MSE signals clearly show a very localized increase in the toroidal current density at the expected location. Further evidence of localized current drive in H–mode plasmas comes from the ECCD stabilization of m/n=3/2 neoclassical tearing modes, which depends sensitively on the current drive being located on the q=3/2 surface [12], where q is the safety factor.

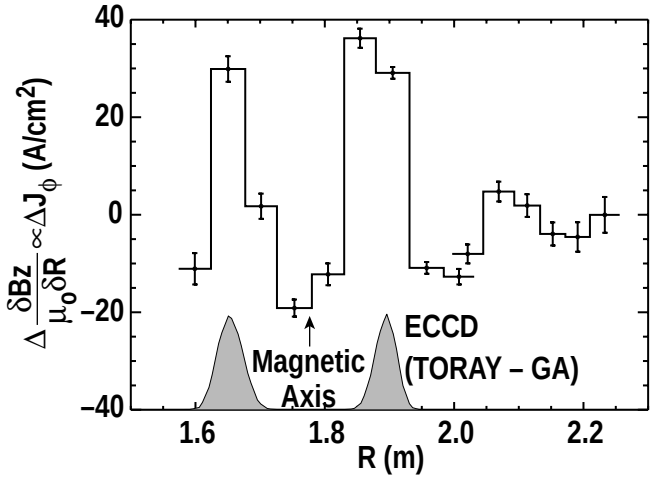

Fig. 2. Measured change in the channel-to-channel differences in the MSE signals between ELMing H–mode discharges with and without ECCD as a function of the major radius. The location and width of the theoretical ECCD profile is also indicated.

CURRENT DRIVE MEASUREMENTS

In this section, some of the important theoretical dependencies of ECCD are tested experimentally on DIII–D, the goal being to validate a predictive model of ECCD. Using the standard theoretical form of the current drive efficiency [13], a dimensionless current drive efficiency can be derived that will be used in this paper [1],

$$\zeta_{ec} = \frac{e^3}{\varepsilon_o^2} \frac{I_{ec} n_e R}{P_{ec} T_e} \tag{3}$$

$$= \quad 3.27\frac{I_{ec}[MA]n_e\left[10^{19}m^{-3}\right]R[m]}{P_{ec}[MW]T_e[keV]} \quad , \tag{4}$$

where I_{ec} is the driven current, and P_{ec} is the ECH power. The ECCD experiments reported in this section have tested several important dependencies of the current drive efficiency by measuring ζ_{ec} as a function of the torodial injection angle ($\propto N_{||}$) as well as some easily varied parameters that effect the electron trapping, such as the normalized radius of absorption (ρ) and electron beta (β). The dependence of ζ_{ec} on the poloidal angle of absorption (Θ_{pol}) has been published previously and showed a systematic increase as the absorption was moved from the low field side to the high field side at constant ρ, owing primarily to reduced trapping effects [3].

Scans of the toroidal injection angle show that the measured ECCD efficiency increases with $N_{||}$, in agreement with theory. This is shown in Fig. 3, where the experimental ECCD is plotted as a function of the toroidal injection angle for a deposition location of ρ = 0.3 and Θ_{pol} = 90° (above the axis). The current drive analysis presented in this paper determines the ECCD profile by directly fitting the MSE signals to a model of the current evolution [3]. Figure 3 shows that the measured ECCD increases from ≈ 0 for radial launch to ≈ 40 kA for co current drive launch at a fixed power of P_{ec} = 1.2 MW. The theoretical ECCD from a quasilinear bounce-averaged Fokker-Planck calculation using the CQL3D code [14], including the effect of the parallel electric field ($E_{||}$), is also given in Fig. 3 and is seen to be in excellent agreement with the measurements. Theoretically, the ECCD is expected to increase with $N_{||}$ because the electron cyclotron waves interact with higher parallel velocity electrons.

For off-axis absorption, the measured ECCD efficiency increases with increasing local electron beta, as shown in Fig. 4. For these experiments, the electron beta is varied by scanning the neutral beam heating power and by utilizing both L–mode and H–mode plasmas. The ECCD is measured at two radial positions, ρ = 0.3 and ρ = 0.4, for $N_{||}$ = 0.4 and Θ_{pol} =90°. In Fig. 4, the experimental ECCD efficiency at ρ = 0.4 increases by nearly a factor of four for an order of magnitude increase in β_e, whereas the increase in ζ_{ec} is a factor 1.5 at ρ = 0.3. At the highest β, the normalized efficiency is about the

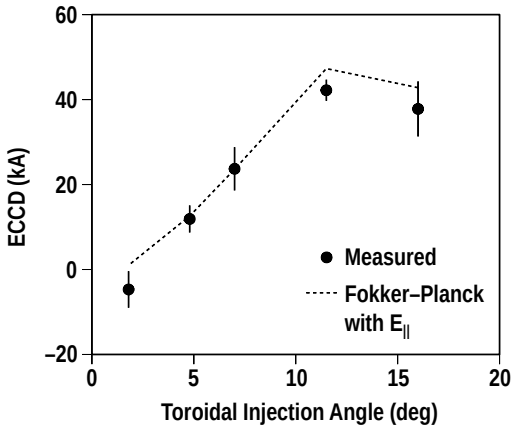

Fig. 3. Dependence of the experimental (filled circles) and theoretical (dashed line) ECCD on the toroidal injection angle of the electron cyclotron waves.

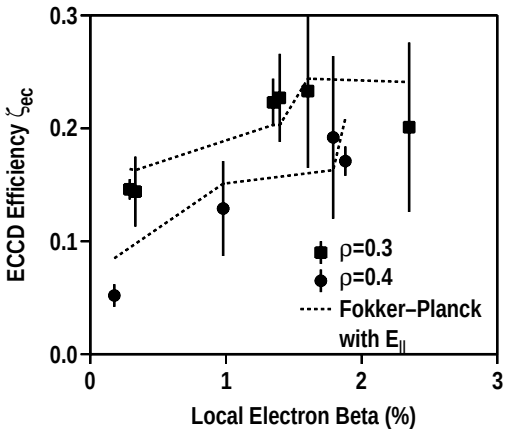

Fig. 4. Measured dependence of the ECCD efficiency on the local electron beta for deposition locations of ρ = 0.3 (squares) and ρ = 0.4 (circles). The theoretical dependence is also shown (dashed lines).

same for $\rho = 0.4$ as for $\rho = 0.3$, indicating that trapping has become nearly negligible. The theoretical ECCD efficiency from the CQL3D Fokker-Planck code, including the effect of $E_{||}$, is also plotted in Fig. 4. The theoretical efficiency is also predicted to increase with β_e, similar to the measurements, although for $\rho = 0.4$ the experimental dependence on β_e appears to be somewhat stronger than predicted.

Theoretically, the increase in ECCD efficiency with increasing electron beta is expected due to reduced electron trapping effects at higher β_e [15]. This explains why the β_e dependence of ECCD is stronger for $\rho = 0.4$ than for $\rho = 0.3$, since the trapped particle fraction increases with minor radius. This theoretical dependence is illustrated in Fig. 5, where the contours of the ECH driven flux in velocity space at $\rho = 0.4$ are shown for both a low-β_e L–mode plasma and a high-β_e H–mode plasma. The ECH driven flux is determined from the CQL3D Fokker-Planck code. The trapped/passing boundary and the ECH resonance are also indicated in this figure. Starting with the $\beta_e = 0.2\%$ case in Fig. 5(a), one can see that there is a small angular separation between the location of the ECH driven flux and the trapped boundary. Therefore, the current carrying electrons can easily be pitch angle scattered into the trapped region of velocity space, which reduces the current drive efficiency. Considering next the β_e=1.8% case in Fig. 5(b), one can see that the ECH resonance has shifted to higher parallel velocities, mainly due to the stronger damping along with relativistic effects, and therefore the resonance is farther from the trapped/passing boundary. In this case, the angular separation between the ECH driven flux and the trapped/passing boundary is greater than for the low-β_e case, and the current carrying electrons are less likely to pitch angle scatter into the trapped region of velocity space. Thus, the electron trapping effects are reduced in high-β_e plasmas, and the ECCD efficiency is correspondently greater.

Off-axis ECCD is more favorable in high-β_e plasmas since the ECCD efficiency does not decrease much with radius. In advanced tokamak scenarios, the ECCD needs to be located at $\rho \approx 0.5$ for current profile control [16]. Since the trapped particle fraction increases with radius, one may expect that the ECCD efficiency should also decrease with radius. Figure 6 shows the measured ECCD efficiency as a function of normalized radius for a low beta L–mode plasma and a high beta H–mode plasma for $N_{||} = 0.4$ and

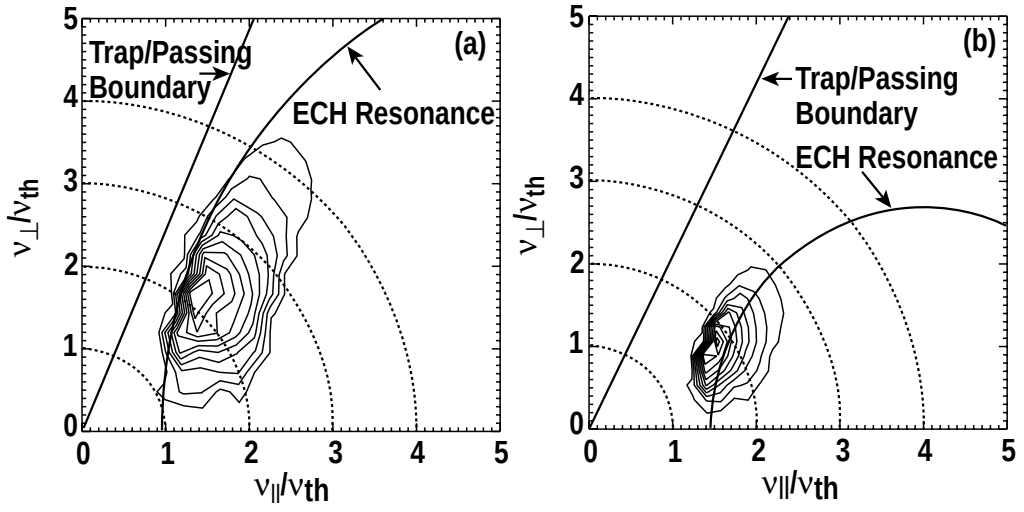

Fig. 5. Contours of ECH driven flux in velocity space at the absorption location for (a) a L–mode plasma with $\beta_e = 0.2\%$, and (b) a H–mode plasma with $\beta_e = 1.8\%$. In this figure, $v_{||}$ is the parallel electron velocity, $v_\perp$ is the perpendicular electron velocity, and v_{th} is the thermal electron velocity. The locations of the trapped/passing boundary and the ECH resonance are also indicated.

Θ_{pol} = 90°. For the L–mode plasma with $<\beta>$ = 0.4%, the experimental ECCD efficiency rapidly decreases with increasing ρ in agreement with theoretical calculations, as has been reported previously [3]. This trend would extrapolate to nearly zero current drive efficiency at $\rho \approx 0.5$. However, Fig. 6 shows that for the H–mode plasma with $<\beta>$ = 2.5%, the experimental ECCD efficiency decreases little with increasing ρ, again in agreement with theoretical calculations. This shows that the detrimental effects of electron trapping on the current drive efficiency are greatly reduced at high β_e. Thus, in high beta plasmas a normalized efficiency of $\zeta_{ec} \approx 0.2$ can be expected at ρ = 0.5, which is what is required for the future advanced tokamak scenarios being developed for DIII–D.

To summarize the current drive results in this section, the measured ECCD on DIII–D is in good agreement with quasilinear Fokker-Planck calculations, including the effect of $E_{||}$, over a wide range of parameters. This is shown in Fig. 7, where the experimental ECCD is compared to the CQL3D code over a wide range of $N_{||}$, Θ_{pol}, β_e, and ρ. The theoretical uncertainties in this figure are due to uncertainties in the launched ECCD power. Figure 7 shows that there is reasonable agreement between theory and experiment for both L–mode and H–mode plasmas. Thus, the DIII–D program is making excellent progress towards experimentally validating a predicted model of ECCD that can be used to plan future applications of current drive for MHD stabilization and current profile control.

CONCLUSIONS

The physics basis for localized, off-axis current drive has been solidified by recent ECCD experiments on the DIII–D tokamak. Very localized absorption and current drive by electron cyclotron waves has been measured in L–mode plasmas for second harmonic X–mode launch from the low magnetic field side of the torus. In H–mode plasmas, experiments modulating the ECH power verify that the wave absorption remains localized to within 10% of the plasma minor radius despite ELMs and the steep edge density gradient. Clear evidence of localized current drive using electron cyclotron waves in H–mode plasmas is seen by MSE spectroscopy. For central deposition, the experimental current drive figure-of-merit is

$$\gamma\left[\mathrm{Am^{-2}W^{-1}}\right] = \frac{I_{ec} n_e R}{P_{ec}} = 0.01 \times 10^{20} \times T_e[\mathrm{keV}] \quad , \tag{5}$$

which corresponds to a dimensionless current drive efficiency of ζ_{ec} = 0.33.

A scan of the toroidal injection angle shows clearly that off-axis ECCD increases with $N_{||}$, with radial injection driving little current. Electron trapping is found to strongly affect the ECCD since the normalized current drive efficiency decreases with increasing radius for low-β_e plasmas. However, for high-β_e plasmas, the ECCD efficiency does not decrease much with increasing radius. This can be explained theoretically by the stronger damping of the electron cyclotron waves with higher density and temperature as well as relativistic effects, causing the ECH resonance to move away from the trapped/passing boundary in velocity space which reduces the deleterious effects of electron trapping and improves the ECCD efficiency. In general, the measured ECCD is in good agreement with quasilinear Fokker-Planck calculations, including the effect of $E_{||}$, over a wide range of parameters. The measured ECCD efficiency for off-axis deposition in high beta H–mode plasmas on DIII–D is equal to the value needed for future advanced tokamak scenarios that will use ECCD for current profile control.

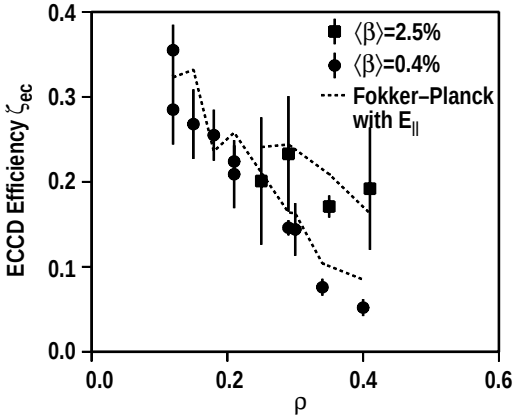

Fig. 6. Experimental ECCD efficiency as a function of the normalized radius of deposition for a L–mode plasma with $<\beta_e>$ = 0.4% (circles) and an H–mode plasma with $<\beta>$ = 2.5% (squares). The theoretical ECCD efficiency is also shown (dashed lines).

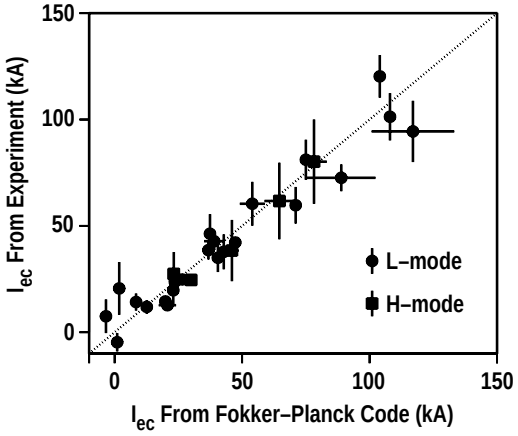

Fig. 7. Comparison of measured and theoretical ECCD over a range of parameters for both L–mode (circles) and H–mode (squares) plasmas.

ACKNOWLEDGMENT

Work supported in part by the U.S. Department of Energy under Contracts DE-AC03-99ER54463, W-7405-ENG-48, and Grant DE-FG03-99ER54541.

REFERENCES

[1] T. C. Luce, *et al*., Phys. Rev. Lett. **83**, 4550 (1999).
[2] T.C. Luce, *et al*.,Plasma Phys. Control. Fusion **41**, B119 (1999).
[3] C.C. Petty, *et al*., Nucl. Fusion **41**, 551 (2001).
[4] V. Erckmann and V. Gasparino, Plasma Phys. Control. Fusion **36**, 1869 (1994).
[5] J. Doane, Int. J. Infrared Millimeter Waves **13**, 1727 (1992).
[6] C.C. Petty, *et al*., Proc. 4th Int. Workshop on Strong Microwaves in Plasmas, Nizhny Novgorod (Russian Academy of Sciences, 2000), p. 41.
[7] Z. Wang, *et al*., Proc. 9th Int. Workshop on Electron Cyclotron Emission and Electron Cyclotron Heating, Borrego Springs (World Scientific, 1995), p. 427.
[8] M. Murakami, *et al.*, Proc. 10th Int. Conf. on Radiofrequency Power in Plasmas, Boston (AIP, 1993), p. 48.
[9] K. Matsuda, IEEE Trans. Plasma Sci. **PS-17**, 6 (1989).
[10] Y.R. Lin-Liu, *et al*., in Proc. 26th Eur. Conf. on Controlled Fusion and Plasma Physics, Maastricht (EPS, 1999), p. 1245.
[11] B.W. Rice, *et al*., Phys. Rev. Lett. **79**, 2694 (1997).
[12] R. Prater, *et al*., Proc. 18th Int. Conf. on Fusion Energy, Sorrento (IAEA, 2000), to be published.
[13] D.A. Ehst and C.F.F. Karney, Nucl. Fusion **31**, 1933 (1991).
[14] R.W. Harvey and M.C. McCoy, Proc. of the IAEA Technical Committee Meeting, Montreal (IAEA, 1993), p. 498.
[15] R. Prater, *et al*., "Decrease in Trapping Effects for Off-Axis Electron Cyclotron Current Drive in High Performance Plasmas," this conference.
[16] C.C. Petty, *et al*., Plasma Phys. Control. Fusion **42**, B75 (2000).